

Ion fluxes through nano-pores and transmembrane channels

J. R. Bordin,¹ A. Diehl,² M. C. Barbosa,¹ and Y. Levin¹

¹*Instituto de Física, Universidade Federal do Rio Grande do Sul
Caixa Postal 15051, CEP 91501-970, Porto Alegre, RS, Brazil*

²*Departamento de Física, Instituto de Física e Matemática,
Universidade Federal de Pelotas, Caixa Postal 354,
CEP 96010-900, Pelotas, RS, Brazil*

(Dated: May 23, 2019)

Abstract

We introduce a new approach for calculating ionic fluxes through narrow nano-pores and transmembrane channels. The method relies on a dual-control-volume grand-canonical molecular dynamics (DCV-GCMD) simulation and the analytical solution for the electrostatic potential inside a cylindrical nano-pore recently obtained by Levin [1]. The theory is used to calculate the ionic fluxes through a gramicidin A channel, obtaining the current-voltage and the current-concentration relations under various experimental conditions. A good agreement with experimental results is observed.

PACS numbers: 87.16.Uv, 87.10.Tf, 87.16.A-

I. INTRODUCTION

Ion channels are water-filled holes, formed when specific proteins are incorporated into the phospholipid membrane [2]. The channels serve to establish an electrostatic potential gradient across the cell membrane by allowing an ion specific flux to pass through the membrane. There are many different ion channels in living cells. These differ in composition, pore structure, and ion selectivity [3, 4]. Thus, a full description of the architecture and operation of ion channels is a very difficult task. From purely electrostatic point of view, operation of ion channels presents an interesting theoretical puzzle. Since the channel passes through a low-dielectric membrane, there exists a large potential energy barrier for ionic solvation inside the pore. Yet, in practice, it is well known that when open, ion channels sustain a very large ionic transport rate, compatible with a free diffusion. There have been a number of different strategies proposed to understand the ion transport across the channel. One approach used extensively over the last few years is all-atom molecular dynamics simulation (MD). The advantage of atomistic MD is that molecular structure of the pore, ionic species, and water are taken explicitly into account [4–7]. Although this method is very appealing, the computational time needed to achieve stationary current is very large [8–10] and, in most cases, is still beyond the available computational resources. Furthermore, the classical water models used in all-atom simulations are parameterized for bulk water and might show erroneous behavior in a strongly confined environment. Such artifacts of classical water and ion models have been recently observed in the studies of ionic solvation near interfaces, when compared to the full *ab initio* simulations [11]. One alternative to atomistic MDs are the, so called, Brownian dynamics simulation (BD) [6, 12, 13]. In these simulations only ionic movement is integrated, while the protein degrees of freedom are held fixed and the water is treated as a uniform dielectric continuum. This significantly reduces the computational cost of the simulation, allowing to access much larger time scale. Nevertheless, BD simulations still requires solution of Poisson partial-differential equation at each new time step of the simulation, making them quite difficult to implement.

Recently, it has been shown that for ionic solvation in an interfacial geometry properly constructed dielectric continuum models agree better with results of full *ab initio* simulations than the classical explicit water models [11, 14, 15]. In the case of a gramicidin channel, MD simulations predicts a potential of mean-force (PMF) with barrier much larger than ex-

pected [10] based on experimental measurements. Thus, in order to avoid the difficulties of all-atom and BD simulations, as well as to be able to explore large time scales necessary for measuring the transmembrane currents, it might be useful to use the dielectric continuum models of ion channels as a first order approximation for the transmembrane dynamics. In this paper we will explore the transmembrane ionic fluxes using the continuum electrostatics model recently introduced by Levin [1]. Briefly stated, Levin solved the Poisson equation with the appropriate boundary conditions to obtain an analytical expression for the electrostatic interaction potential (Green function) between the charges inside a finite cylindrical pore passing through a low-dielectric phospholipid membrane. This electrostatic potential can be used to calculate the forces acting between the ions inside the pore and between the ions and the charged protein residues embedded in the cell membrane. In this paper, we will use the interaction potential derived by Levin in a series of Dual-Control-Volume Grand-Canonical Molecular Dynamics (DCV-GCMD) [16, 17] simulations of a gramicidin A (gA) channel. The gA channel is a polypeptide with an alternating L-D-amino acid sequence [10, 18] which fold as a helix. Its cylindrical shape is formed by monomeric β -helices joined by hydrogen bonds in the NH_2 terminal, whose atomic structure is known in great detail [19–24]. One of the most striking features of such linear structure is the high ion valence selectivity of the gA channel, since in general only monovalent cation flux is observed [25, 26]. The main advantage of using the gA channel is the wealth of information on the ion permeability for different concentrations and applied voltages that is available [27–31]. In the present paper we will explore using the DCV-GCMD the flow of ionic current through the gA channel for different electrolyte concentrations and externally applied electric fields. We should stress that our model is very different from the mean-field Poisson-Nernst-Planck (PNP) theory [32, 33], where the Poisson equation and the continuity equations for mobile ions are solved simultaneously in a self-consistent way. For narrow channel such as gA the correlational effects between the ions are of fundamental importance and the mean-field description of ionic conduction is bound to fail [34].

The paper is organized as follows. The model and computational details are given in Sec. II. The results are discussed in Sec. III and the summary and conclusions are presented in Sec. IV.

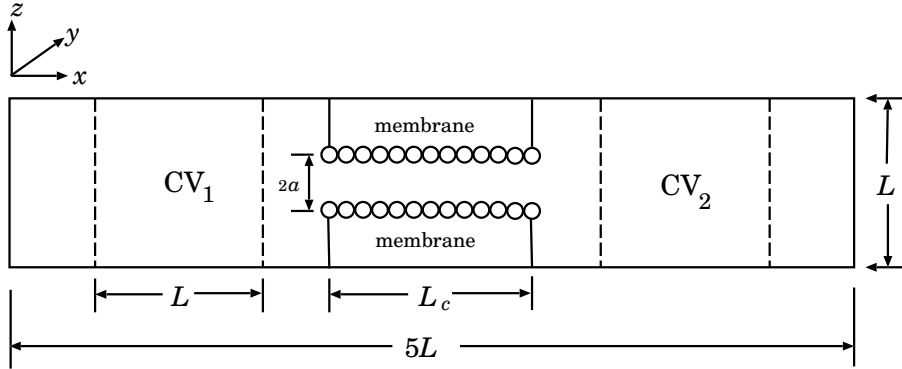


FIG. 1: Schematic depiction of the simulation cell.

II. THE MODEL SYSTEM AND THE SIMULATION METHODOLOGY

A. A model for ion channels

We will use the channel-reservoir setup illustrated schematically in Fig. 1 to calculate the ionic currents due to concentration and electrostatic potential gradients. The simulation box, a cubic parallelepiped with volume $5L \times L \times L$ and $L = 20 \text{ \AA}$, contains two reservoirs (two control volumes CV_1 and CV_2 , within which the chemical potentials of the ionic species are maintained constant) and a membrane with a channel connecting these two reservoirs. The channel structure, a simplified model of a gramicidin A pore, is built as a cylindrical tube, with radius $a = 3 \text{ \AA}$ and length $L_c = 35 \text{ \AA}$, made of stationary Lennard-Jones (LJ) spheres of diameter $\sigma_c = 2 \text{ \AA}$. Both sides of the channel structure — except for the orifices — are bound by confining walls, as well as the two extremes of the simulation box in the x direction, see Fig. 1. The system contains positive and negative ions with diameters σ_+ and σ_- , respectively, inside a structureless solvent of dielectric constant $\epsilon_w = 80$ — the same value of dielectric is used inside and outside the channel — while the membrane has a dielectric constant equals to $\epsilon_m = 2$, both in units of vacuum permittivity. The particle-particle interactions are separated into short and long-range contributions, while the particle-channel has only a short-range interaction. For the short-range part we will use the WCA LJ potential [35]

$$U_{ij}^{\text{WCA}}(r) = \begin{cases} U_{\text{LJ}}(r) - U_{\text{LJ}}(r_c), & r \leq r_c, \\ 0, & r > r_c, \end{cases} \quad (1)$$

where $U_{LJ}(r)$ is the standard 12-6 LJ potential. The cut-off distance is $r_c = 2^{1/6}\sigma_{ij}$, where $\sigma_{ij} = (\sigma_i + \sigma_j)/2$ is the center-to-center separation between an ion of species i (cation or anion) and a particle of species j (cation, anion, or a fixed LJ channel sphere) separated by a distance r . The confining walls in simulation box extremes and surrounding the channel structure are modeled with the same WCA LJ potential, however considering the x -projection of the distance between one ion in the bulk and the wall position.

The long-range contribution is calculated depending on the region where the ion is located. For the regions outside the channel, the interaction energy between the two ions is the usual Coulomb potential

$$U_{ij}^{\text{coul}}(r) = \frac{1}{4\pi\epsilon_w} \frac{q_i q_j}{r_{ij}}, \quad (2)$$

where r_{ij} is the distance between the two ions. The infinite extent of the particle reservoir is taken into account using the Ewald summation.

For the region inside the channel we will use the model introduced by Levin [1]. In this model ions inside the pore interact through the electrostatic potential which is only a function of their separation in the x -direction (along the axis of symmetry of the channel). This is quite reasonable for narrow channels such as gA. When one ion with charge q enters into the channel it interacts with the other ions and with the p residues of charge $-q$ embedded into the channel wall at transverse distance ρ from the central axis. In addition to the electrostatic interaction between the ions and the residues, there is a self-energy penalty U associated with an ion entering into the region surrounded by the low-dielectric material. The electrostatic energy of the ions inside the pore is then

$$V = \frac{1}{2} \sum_{i=1}^N \sum_{j=1}^N q_i \varphi_{\text{in}}(x_i, x_j) + \sum_{i=1}^N \sum_{j=1}^p q_i \varphi_{\text{out}}(x_i, \rho, x_j) + \sum_{i=1}^N q_i U(x_i), \quad (3)$$

where $\varphi_{\text{in}}(x_i, x_j) = \varphi_1(x_i, x_j) + \varphi_2(x_i, x_j)$. The two electrostatic potentials are [1]

$$\varphi_1(x_i, x_j) = \frac{q}{\epsilon_w} \int_0^\infty dk \frac{\{\alpha^2(k)e^{k|x_i-x_j|-2kL_C} + \alpha(k)\beta(k)[e^{-k(x_i+x_j)} + e^{k(x_i+x_j)-2kL_C}] + \beta^2(k)e^{-k|x_i-x_j|}\}}{\beta^2(k) - \alpha^2(k) \exp[-2kL_C]}, \quad (4)$$

where $\alpha = [k - (k^2 + \kappa^2)^{1/2}]$ and $\beta = [k + (k^2 + \kappa^2)^{1/2}]$, with κ the inverse Debye length that characterizes the electrolyte concentration in the two reservoirs, and

$$\varphi_2(x_i, x_j) = \frac{4q(\epsilon_w - \epsilon_p)}{\epsilon_w L_C} \sum_{n=1}^{\infty} \frac{K_0(k_n a) K_1(k_n a) \sin(k_n x_i) \sin(k_n x_j)}{\epsilon_w I_1(k_n a) K_0(k_n a) + \epsilon_p I_0(k_n a) K_1(k_n a)}, \quad (5)$$

where I_n and K_n are the modified Bessel functions of order n . Here a is the channel radius and $k_n = n\pi/L_c$. The interaction potential between an ion and a fixed charged residue is

$$\varphi_{\text{out}}(x_i, \rho, x_j) = \frac{4q}{L_c} \sum_{n=1}^{\infty} \frac{1}{k_n a \epsilon_w I_1(k_n a) K_0(k_n a) + \epsilon_p I_0(k_n a) K_1(k_n a)} \frac{K_0(k_n \rho) \sin(k_n x_i) \sin(k_n x_j)}{.} \quad (6)$$

Finally, the electrostatic barrier is given by

$$U(x) = \frac{q}{2\epsilon_w} \int_0^{\infty} dk \frac{\{2\alpha^2(k)e^{-2kL_c} + \alpha(k)\beta(k)[e^{-2kx} + e^{2k(x-L_c)}]\}}{\beta^2(k) - \alpha^2(k) \exp[-2kL_c]} + \frac{2q(\epsilon_w - \epsilon_p)}{\epsilon_w L_c} \sum_{n=1}^{\infty} \frac{K_0(k_n a) K_1(k_n a) \sin^2(k_n x)}{\epsilon_w I_1(k_n a) K_0(k_n a) + \epsilon_p I_0(k_n a) K_1(k_n a)} + \frac{q\kappa}{2\epsilon_w}. \quad (7)$$

Based on experimental and theoretical results [6, 10, 23], we have placed two residues of charge $-q$ each embedded into the channel wall ($\rho = 3 \text{ \AA}$) at positions $x = -10.5 \text{ \AA}$ and $x = 10.5 \text{ \AA}$, to represent the two binding sites of the gramicidin A channel.

B. Simulation details

Gramicidin A channels are highly selective to cation passage. Although the actual transport process is very complicated, we can identify three main steps [10]: (1) cation entry, where the positive ions are dehydrated by polar groups in the pore walls, (2) cation translocation through the channel, and (3) cation exit. Since in our model we do not consider water molecules explicitly, we simulate step (1) above using a ‘‘partially-dehydrated’’ diameter for the cations equals to $\sigma_+ = 2 \text{ \AA}$, while the negative ions have a ‘‘hydrated’’ diameter $\sigma_- = 4 \text{ \AA}$. Since the channel is very narrow, the available radius for ion movement is approximately $a - \sigma_c/2$ in Fig. 1. Therefore, using these diameters only positive ions can enter into the channel. In all interactions the energy parameter of LJ potential was defined as $\epsilon = 1k_B T$. During the MD steps, we have used Langevin dynamics to simulate the effect of solvent on the cation and anion movement, solving the equation of motion of ion i ,

$$m_i \vec{a}_i = \vec{F}_i - m\gamma \vec{v}_i + \vec{W}(t), \quad (8)$$

where \vec{F}_i is the total force on ion i due to all entities explicitly present in the model (other ions, protein residues, and walls), γ is the friction coefficient, and $\vec{W}(t)$ is the random force [36] due to solvent. The temperature of the system is maintained constant using the fluctuation-dissipation theorem,

$$\langle \vec{W}(t) \cdot \vec{W}(t') \rangle = 6k_B T \gamma \delta(t - t'), \quad (9)$$

which relates the friction coefficient to the fluctuations of the random force using the appropriate γ value. In our simulations we have used $m_i = 6.5 \times 10^{-26}$ kg, corresponding to the mass of K^+ ion; $\gamma^{-1} = 53$ fs for the region outside the channel, corresponding to diffusion constant $D = k_B T / m_i \gamma$ of $D = 3.37 \times 10^{-9}$ m²/s; and $\gamma_c^{-1} = \gamma^{-1}/3$ inside the channel corresponding to diffusion constant of $D = 1.12 \times 10^{-9}$ m²/s. These values were chosen in order to maintain the temperature fixed at 298 K and to reproduce the experimental behavior, particularly the saturation observed in the current-concentration curves [6].

The concentrations in both reservoirs are maintained constant using DCV-GCMD simulations [16, 17, 37–41]. Briefly stated, in the DCV-GCMD simulation two control volumes (CV) are initially prepared at desired concentrations using the grand canonical Monte Carlo (GCMC) simulation and then evolved in time using the molecular dynamics (MD) simulation. Since the dynamics alters the CV concentrations, the MD steps are intercalated with the grand canonical Monte Carlo (GCMC) simulations performed inside the two control volumes (CV) shown in Fig. 1. This restores the concentrations to their initial values. In our simulations we have used 50 GCMC steps for every 500 MD steps.

Since our simulation setup is periodic only in two directions, as shown in Fig. 1, for the long-range interactions described by Eq. (2) we have used the Ewald summation with the implementation of Yeh and Berkowitz [42] for the slab geometry. The equations of motion were integrated using the velocity Verlet algorithm, with a time step of 8.0 fs in the MD simulations. The observables were obtained using 5 to 10 independent realizations.

III. RESULTS AND DISCUSSION

We start our discussion with the two CVs having the same concentration and the ionic diffusion through the gA channel driven by externally imposed electrostatic potential gradient. We are particularly interested in the current-voltage and current-concentration curves and their comparison with the experimental results, mainly the appearance of the experimentally observed saturation in the current-concentration profiles. In Fig. 2 we show the current-voltage curve for the concentration of 0.5 M in both CVs. As one can see, the expected linear dependence between the ionic current and applied voltage was obtained in a good agreement with the experimental and earlier BD simulations [6].

Next we analyze the behavior of the current-concentration profiles for two externally

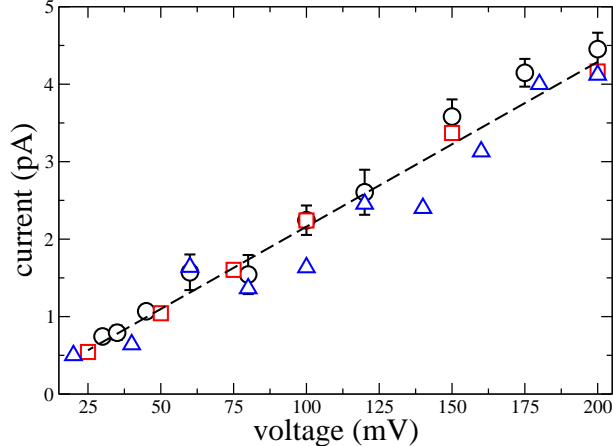


FIG. 2: Current-voltage curve for 0.5 M concentration of electrolyte in both CVs. Open circles are our simulations results. The open squares and the open triangle are the experimental and BD results, respectively, extracted from Fig. 12 of Ref. [6].

applied voltages of 100 mV and 200 mV, Fig. 3. Again we find a good agreement with experimental and BD simulation results [6]. In particular we see the saturation of the ionic current observed experimentally. For 200 mV and above 0.9 M concentration, however, we find some deviation from the experimental results. The deviation appears to be an artifact of including only 30 terms in the infinite series of the electrostatic potential inside the cell, Eqs. (5) and (6). Cutting the infinite series at only 30 terms softens the repulsion between the ions inside the channel favoring an increased flux.

Experimental [20, 21, 24, 43] and BD simulations [6] data have proposed two large concentration peaks at the binding sites separated by a cation depleted region. This is exactly what we observe in our simulations, as shown in Fig. 4 for 0.5 M monovalent solution in both CVs with no voltage or with 200 mV applied potential difference.

To understand better the mechanism of ionic translocation, in Fig. 5 we plot the electrostatic potential inside the gA channel Eq. (3) at zero applied voltage. If the channel has no fixed residues, equation (7) leads to a large electrostatic potential energy barrier of approximately $8 k_B T$, which prevents any cation entrance. On the other hand, if the protein has charged residues embedded into the surface of the channel, the scenario changes completely. As one can see, with no cation inside the channel we have an energy barrier of approximately $4 k_B T$ separating two deep wells at the positions of the binding sites. The

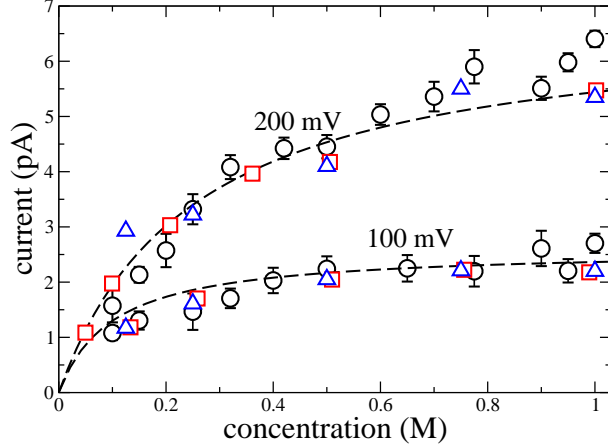


FIG. 3: Current-concentration curves for external voltages of 100 mV and 200 mV. Our simulations are represented by open circles. The open squares and open triangles are the experimental and BD results, respectively, extracted from Fig. 12 of Ref. [6].

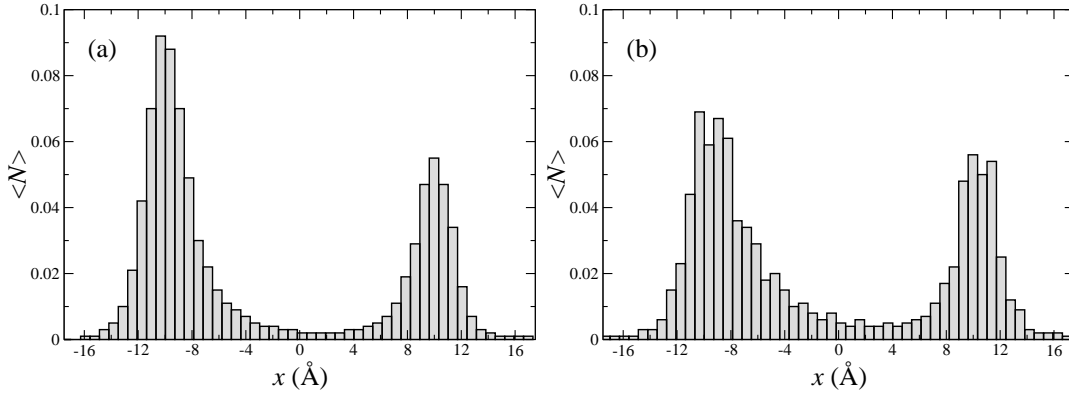


FIG. 4: Mean number of cations in the axial direction of gA channel with (a) no applied voltage and (b) 200 mV applied potential. In both cases there is 0.5 M monovalent electrolyte solution in the two CVs.

entrance of a cation alters drastically the potential energy landscape. Suppose that one ion is already inside the channel. We are interested in the potential of mean-force (PMF) that a second ion will feel as it moves through the channel. This PMF is plotted as a dashed curve in Fig. 5. A short time after the first ion's entrance into the channel its most probable location is at the first binding site. Thus, when the second ion enters the channel, it sees the field of attractive residue partially screened by the first ion, so that the depth of the

potential well produced by the first residue is significantly smaller. As the second ion moves farther into the channel, it forces the first ion to move to the second residue, and eventually to completely leave the channel. If at $t=0$ there are two ions in the channel, their most probable location will be at the two residues. The third ion will then encounter a flat energy landscape shown in Fig. 5 by a dotted curve. This then explains the fast transport of ions through the ion channel observed experimentally. In the BD studies [6] the saturation was forced by postulating a fixed double well potential of depth of $8 k_B T$ and a barrier between the wells of $5 k_B T$. In the present study, the electrostatic energy landscape is calculated self-consistently, without any adjustments.

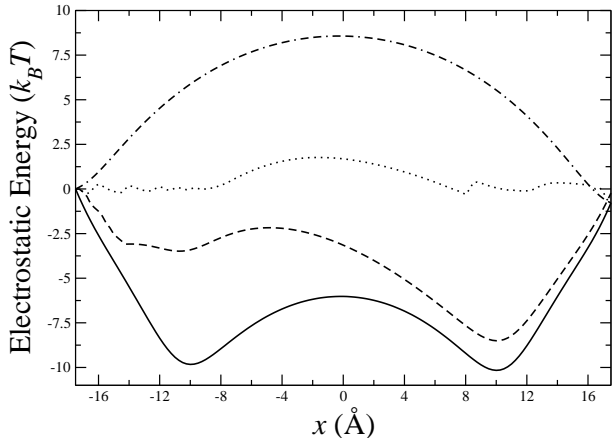


FIG. 5: Potential energy profile inside a gA channel obtained from Levin’s model [1]. The curves show the potential of mean force (PMF) felt by an ion moving through a gA channel with two residues located at $x = -10.5 \text{ \AA}$ and $x = +10.5 \text{ \AA}$ (solid line). The PMF if the channel already has a free cation near the first binding site is represented by a dashed line, while the PMF if there are already two free cations near the two binding sites is represented by a dotted line. The dot-dashed line represents the electrostatic barrier produced by Eq. (7). The concentration in the CVs is 0.5 M with no applied voltage.

In Fig. 6 we show the distribution of times of cation translocation through the channel for voltage difference of 100 mV and CV concentration of 0.5 M. The mean first passage time (MFPT) as a function of applied voltage and CVs concentration is also shown in Fig. 6. The saturation observed in Fig. 3 can also be seen in the MFPT results.

We finish our discussion by presenting the cationic current as a function of concentration gradient between the two CVs. This is done in DCV-GCMD simulation by fixing the con-

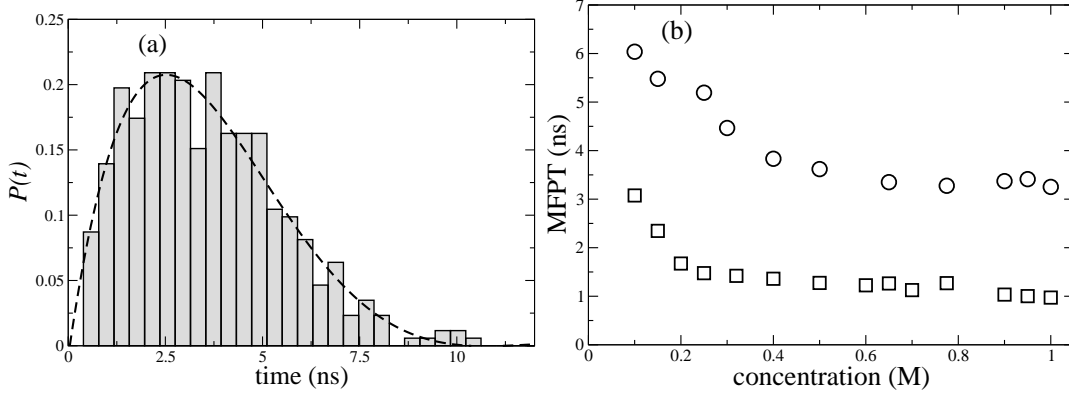


FIG. 6: (a) Distribution of passage time $P(t)$ for 100 mV applied voltage and CV concentration of 0.5 M. (b) Mean first passage time (MFPT) as a function of CV concentrations for 100 mV (open circles) and 200 mV (open squares) applied voltages.

concentration of CV_2 at $C_2 = 0.4$ M and using CV_1 concentrations ranging from $C_1 = 0.5$ M to $C_1 = 1$ M, with the concentration gradient defined as $\Delta C = C_1 - C_2$. Since the interaction potential is not very sensitive to the precise value of κ we have simply used the average concentration in the two reservoirs to calculate the inverse Debye length. The results are shown in Fig. 7. Unlike the current-voltage curve shown in Fig. 2, we obtain a non-linear dependence between the cationic current and the concentration gradient between the two CVs.

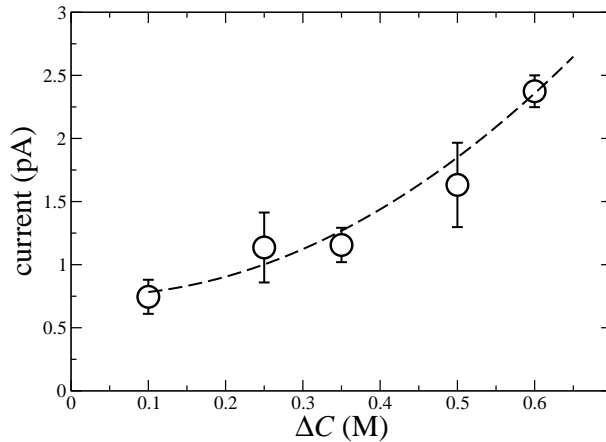


FIG. 7: Cationic current as a function of the concentration gradient between the two CVs with no external voltage.

IV. CONCLUSIONS

We have used a Dual-Control-Volume Grand-Canonical Molecular Dynamics (DCV-GCMD) simulations to study the flow of ions through the narrow pores across a low dielectric membrane. To account for the electrostatic interactions inside the channel we used the analytical potentials recently derived by Levin [1]. For electrolyte concentrations of up to 1 M our simulations show a good agreement with the experimental measurements of ionic current as a function of both electrostatic potential difference and concentration. To obtain reliable results for larger concentrations one must include more terms in the infinite series for the ion-ion interaction potential. For physiological concentrations of electrolyte the continuum model presented in this work appears to show excellent agreement with the experimental measurements. The utility of the model is that the simulations do not require expensive computational resources and can be run on a desktop PC. One interesting application of the model is to study the dependence of ionic current on mutations of charged residues — the position and the charge of the residues that enter into the electrostatic potential can be optimized to obtain the desirable channel characteristics. This could be of interest for design and implementation of molecularly engineered ion channels and nano-pores.

V. ACKNOWLEDGEMENTS

This work was partially supported by the CNPq, Capes, Fapergs, INCT-FCx, and by the US-AFOSR under the grant FA9550-09-1-0283.

-
- [1] Y. Levin. *Europhys. Letters*, **76**, 163 (2006).
 - [2] B. Hille. *Ion channels of excitable membranes (third ed.)*. Mass: Sinauer Associates, Sunderland, 2001.
 - [3] D. A. Doyle, J. M. Cabral, R. A. Pfuetzner, A. Kuo, J. M. Gulbis, S. L. Cohen, B. T. Chait, and R. MacKinnon. *Nature* **280**, 5360 (1998).
 - [4] S. Berneche and B. Roux. *Nature* **414**, 73 (2001).
 - [5] B. Roux. *Biophys. J.* **71**, 3177 (1996).
 - [6] S. Edwards, B. Corry, S. Kuyucak, and S. Ho Chung. *Biophysical J.* **83**, 1348 (2002).

- [7] B. Roux, T. W. Allen, T. W. Bernèche, and W. Im. *Q. Rev. Biophys.* **37**, 15 (2004).
- [8] D. G. Levitt. *J. Gen. Physiol.* **113**, 789 (1999).
- [9] B. Roux. *Curr. Opin. Struct. Biol.* **12**, 182 (2002).
- [10] O. S. Andersen, R. E. Koeppe, and B. Roux. *IEEE Trans. Nanobiosci.* **4**, 10 (2005).
- [11] M. D. Baer and C. J. Mundy. *J. Phys. Chem. Lett* **2**, 1088 (2011).
- [12] G. Moy, B. Corry, S. Kuyucak, and S. H. Chung. *Biophys. J.* **78**, 2349 (2000).
- [13] B. Corry, S. Kuyucak, and S. H. Chung. *Biophys. J.* **78**, 2364 (2000).
- [14] Y. Levin, A. P. dos Santos, and A. Diehl. *Phys. Rev. Lett.* **103**, 257802 (2009).
- [15] A. P. dos Santos, A. Diehl, and Y. Levin. *Langmuir* **26**, 10778 (2010).
- [16] G. S. Heffelfinger and F. Van Smol. *J. Chem. Phys.* **100**, 7548 (1994).
- [17] A. P. Thompson, D. M. Ford, and G. S. Heffelfinger. *J. Chem. Phys.* **109**, 6406 (1998).
- [18] R. Sarges and B. Witkop. *J. Amer. Chem. Soc.* **87**, 2011 (1965).
- [19] D. W. Urry, K. U. Prasad, and T. L. Trapane. *Proc. Natl Acad. Sci. USA* **79**, 390 (1982).
- [20] D. W. Urry, T. L. Trapane, C. M. Venkatachalam, and R. B. McMichens. *Methods Enzymol.* **171**, 286342 (1989).
- [21] G. A. Olah, H. W. Huang, W. Liu, and Y. Wu. *J. Mol. Biol* **218**, 847 (1991).
- [22] N. Jing, K. U. Prasad and D. W. Urry. *Biochimica et Biophysica Acta* **1238**, 1 (1995).
- [23] R. R. Ketchum, B. Roux, and T. A. Cross. *Structure* **5**, 1655 (1997).
- [24] F. Tian and T. A. Cross. *J. Mol. Biol.* **285**, 1993 (1999).
- [25] D. G. Levitt, S. R. Elias, and J. M. Hautmann. *Biochim. Biophys. Acta* **512**, 436 (1978).
- [26] O. S. Andersen. *Annu. Rev. Physiol.* **46**, 531 (1984).
- [27] E. Neher and J. Sandblom and. G. Eisenman. *J. Membrane Biol.* **40**, 97 (1978).
- [28] C. D. Cole, A. S. Frost, N. Thompson, M. Cotten, T. A. Cross, and D. D. Busath. *Biophys. J.* **83**, 1974 (2002).
- [29] D. D. Busath, C. D. Thulin, R. W. Hendershot, L. R. Phillips, Peter Maughan, C. D. Cole, N. C. Bingham, S. Morrison, L. C. Baird, R. J. Hendershot, M. Cotten, and T. A. Cross. *Biophys. J.* **75**, 2830 (1998).
- [30] M. D. Becker, R. E. Koeppe II, and O. S. Andersen. *Biophys. J.* **62**, 25 (1992).
- [31] A. E. Cárdenas, R. D. Coalson, and M. G. Kurnikova. *Biophys. J.* **79**, 80 (2000).
- [32] R. S. Eisenberg. *J. Membr. Biol.* **171**, 1 (1999).
- [33] D. G. Luchinsky, R. Tindjong, I. Kaufman, P. V. E. McClintock, and R. S. Eisenberg. *Phys.*

- Rev. E* **80**, 021925 (2009).
- [34] Y. Levin, *Rep. Prog. Phys.* **65**, 1577 (2002).
- [35] M. P. Allen, and D. J. Tildesley. *Computer Simulation of Liquids*. Oxford University Press, Oxford, 1987.
- [36] N. Wiener. *J. Math. and Phys.* **2**, 131 (1923).
- [37] A. V. Raghunathan, and N. R. Aluru. *Phys. Rev. E* **76**, 011202 (2007).
- [38] G. S. Heffelfinger, and D. M. Ford. *Mol. Phys.* **94**, 659 (1998).
- [39] G. S. Heffelfinger, and D. M. Ford. *Mol. Phys.* **94**, 673 (1998).
- [40] P. I. Pohl, and G. S. Heffelfinger. *J. Membrane Sci.* **155**, 1 (1999).
- [41] M. Horsch, and J. Vrabec. *J. Chem. Phys.* **131**, 184104 (2009).
- [42] M. L. Berkowitz and I. Yeh. *J. Chem. Phys.* **111**, 3155 (1999).
- [43] L. V. Schagina, A. E. Grinfeldt, and A. A. Lev. *Nature* **273**, 243 (1978).